

# Scaling analysis of a divergent prefactor in the metastable lifetime of a square-lattice Ising ferromagnet at low temperatures

Kyungwha Park<sup>1,\*</sup>, M. A. Novotny<sup>2,†</sup>, P. A. Rikvold<sup>1,3,‡</sup>

<sup>1</sup>*School of Computational Science and Information Technology, Florida State University,  
Tallahassee, Florida 32306*

<sup>2</sup>*Department of Physics and Astronomy, Mississippi State University, Mississippi State,  
Mississippi 39762*

<sup>3</sup>*Center for Materials Research and Technology and Department of Physics, Florida State  
University, Tallahassee, Florida 32306*

(December 2, 2024)

## Abstract

We examine a square-lattice nearest-neighbor Ising quantum ferromagnet coupled to  $d$ -dimensional phonon baths. Using the density-matrix equation, we calculate the transition rates between configurations, which determines the specific dynamic. Applying the calculated stochastic dynamic in Monte Carlo simulations, we measure the lifetimes of the metastable state. As the magnetic field approaches  $|H|/J = 2$  at low temperatures, the lifetime prefactor diverges because the transition rates between certain configurations approaches zero at these conditions. Near  $|H|/J = 2$  and zero temperature, the divergent prefactor shows scaling behavior as a function of the field, temperature, and the dimension of the phonon baths. With proper scaling, the simulation data at different temperatures and for different dimensions of the baths collapse well onto two master curves, one for  $|H|/J > 2$  and one for  $|H|/J < 2$ .

PACS numbers:64.60.Qb,75.60.Jk,05.50.+q,02.50.Ga

## I. INTRODUCTION

Compared to the exponents of particular physical quantities, the associated prefactors are often assumed to be too unremarkable and uninteresting to examine, so that the study of prefactors has been ignored in many cases. However, this is not always true. In this paper, we explore interesting behavior shown by the prefactors of the lifetime of the metastable state of a two-dimensional nearest-neighbor Ising ferromagnet interacting with phonon baths. Metastability occurs often in many different systems, ranging from supercooled fluids and vapors [1,2] to spin systems [3] and quantum liquids [4]. In those systems some type of weak noise (for example, thermal noise) can drive the system from the metastable state to the stable state across a saddle point at an extremely small rate. Therefore, the average waiting time before escape from a metastable state is usually extremely long.

Recently, we examined a square-lattice Ising quantum ferromagnet with a phonon (i.e., bosonic) bath attached to each spin, in the presence of a longitudinal magnetic field [5,6]. The time evolution of the spin system is determined by the linear coupling of the system with the phonon baths, and the dynamic (defined by the transition rates between different spin configurations) is calculated using the quantum-mechanical density-matrix equation. The resulting dynamic is different from the Glauber dynamic [7], which can be derived in a similar way from coupling with fermionic baths [8]. In the present paper, the calculated transition rates are applied in dynamic Monte Carlo simulations in order to measure the lifetimes of the metastable state. To measure the lifetimes, the initial configuration is set to be all spins up, and a magnetic field which favors all spins down is applied. Then the number of spin-flip attempts is measured until the system magnetization reaches zero. At a particular value of the magnetic field,  $|H|/J = 2$  where  $J$  is the nearest-neighbor exchange coupling constant, the present dynamic does not allow transitions between certain configurations, which causes the lifetime to diverge as the temperature approaches zero and  $|H|/J \rightarrow 2^\pm$ . Since the energy barrier between the stable and metastable states is finite, this means that the prefactor of the lifetime must diverge as  $|H|/J \rightarrow 2^\pm$ . If the Glauber dynamic is applied to the system

instead, then the lifetime prefactor has a finite, field-independent value for  $|H|/J > 2$ , which is different from that for  $|H|/J < 2$  [9,10]. Consequently, the divergence of the prefactor is due to the specific dynamic imposed on the spin system. From the dynamic Monte Carlo simulations, we demonstrate that this divergent prefactor reveals a scaling behavior which is determined by  $T^d$  and the ratio  $(|H| - 2J)/(k_B T)$ , where  $T$  is the absolute temperature and  $d$  is the dimension of the phonon baths.

Quite recently, Maier and Stein investigated the effects of weak noise on the magnetization reversal rate in an overdamped one-dimensional classical Ginzburg-Landau model of finite length [11]. There is no applied field in their model, so thermal fluctuations drive the system from one stable configuration (magnetization near  $+1$ ) to another (magnetization near  $-1$ ) through a saddle point. They analytically calculated the prefactor of the magnetization reversal rate, and found that the rate prefactor diverges as the system size  $L$  reaches  $\pi$  or  $2\pi$ , depending on the boundary conditions. A similar prefactor divergence occurs in a two-dimensional nonequilibrium model [12]. Shneidman and Nita [13] studied a metastable lattice-gas model with nearest-neighbor interactions and continuous-time Metropolis dynamics. They calculated analytically the prefactor of the lifetime of the metastable state beyond the zero-temperature limit. The lifetime prefactor exhibited distinctive peaks as a function of field, which disappear at zero temperature.

The remainder of this paper is organized as follows. In Sec. II we describe our dynamic quantum model, and in Sec. III we show how to calculate the prefactor analytically and numerically. In Sec. IV we present our scaling analysis of the prefactor, and in Sec. V we present a discussion and our conclusions.

## II. DYNAMIC QUANTUM MODEL

To derive the classical dynamic (i.e., transition rates) from the quantum system, we use the Hamiltonian:

$$\mathcal{H} = \mathcal{H}_{\text{sp}} + \mathcal{H}_{\text{ph}} + \mathcal{H}_{\text{sp-ph}} , \quad (1)$$

$$\mathcal{H}_{\text{sp}} = -J \sum_{\langle i,j \rangle} \sigma_i^z \sigma_j^z - H_z \sum_i \sigma_i^z , \quad (2)$$

$$\mathcal{H}_{\text{ph}} = \sum_q \hbar \omega_q c_q^\dagger c_q , \quad (3)$$

$$\mathcal{H}_{\text{sp-ph}} = \lambda \sum_{j,q} \sqrt{\frac{\hbar}{2NM\omega_q}} (iq \sigma_j^x) (c_q^\dagger - c_q) e^{iqR_j} , \quad (4)$$

where  $\mathcal{H}_{\text{sp}}$  is the spin Hamiltonian,  $\mathcal{H}_{\text{ph}}$  is the phonon Hamiltonian, and  $\mathcal{H}_{\text{sp-ph}}$  [14] is the Hamiltonian describing the simple linear spin-phonon coupling. The first sum in Eq. (2) runs over nearest-neighbor sites only on a two-dimensional square lattice,  $J(> 0)$  is the ferromagnetic exchange coupling constant,  $\sigma_j^z$  are the  $z$  components of Pauli spin operators attached to lattice site  $j$ , and  $H_z$  is a longitudinal magnetic field. The index  $q$  is the wave vector of a phonon mode,  $\omega_q$  is the angular frequency of the phonon mode with wave vector  $q$ , and  $c_q^\dagger$  and  $c_q$  are the corresponding creation and annihilation operators. The constant  $\lambda$  (its dimension is energy) is the coupling strength between the spin system and the phonon heat bath,  $N$  is the number of unit cells in the system,  $M$  is the mass per unit cell, and  $R_j$  is the position of site  $j$ . Details of this model were presented in Refs. [5,6], and thus here we only briefly sketch the main ideas.

With the given spin Hamiltonian, the dynamic is determined by the generalized master equation [15,16]:

$$\begin{aligned} \frac{d\rho(t)_{m'm}}{dt} &= \frac{i}{\hbar} [\rho(t), \mathcal{H}_{\text{sp}}]_{m'm} + \delta_{m'm} \sum_{n \neq m} \rho(t)_{nn} W_{mn} \\ &\quad - \gamma_{m'm} \rho(t)_{m'm} , \\ \gamma_{m'm} &= \frac{W_m + W_{m'}}{2} , \quad W_m = \sum_{k \neq m} W_{km} , \end{aligned} \quad (5)$$

where  $\rho(t)$  is the time dependent density matrix of the spin system,  $m'$ ,  $n$ ,  $k$ , and  $m$  are eigenstates of  $\mathcal{H}_{\text{sp}}$ ,  $\rho(t)_{m'm} = \langle m' | \rho(t) | m \rangle$ , and  $W_{km}$  is the transition rate from the  $m$ th to the  $k$ th eigenstate. Assuming that the correlation time of the heat bath is much smaller than the times of interest, we integrate over all degrees of freedom of the bath. Then the transition rate from the  $m$ th to the  $k$ th eigenstate of  $\mathcal{H}_{\text{sp}}$  becomes [5,6]

$$W_{km} = \frac{\lambda^2}{\Theta \eta \hbar^{d+1} c^{d+2}} \left| \frac{(E_k - E_m)^d}{e^{\beta(E_k - E_m)} - 1} \right| , \quad (6)$$

where  $d$  is the dimension of the heat bath,  $\Theta = 2$  ( $2\pi$ ) for  $d = 1, 2$  ( $3$ ),  $\eta = M/a^d$  where  $a$  is the lattice constant,  $c$  is the sound velocity, and  $\beta = 1/k_B T$ . The two major differences from the Glauber dynamic are the energy difference term in the numerator and the negative sign in the denominator. In the limit  $T \rightarrow 0$ , the transition rates vanish when  $E_m = E_k$  (this can occur for  $|H| = 2J, 4J$ ). Despite their unusual form, these transition rates satisfy detailed balance. The transition rates for different  $d$  scaled by  $(k_B T)^d$  are shown in Fig. 1(a) as a function of  $\beta(E_k - E_m)$ . This can be compared with the transition rate for the Glauber dynamic, shown in Fig. 1(b).

### III. PREFACTOR: THEORY AND SIMULATION

We apply the calculated transition rates for the  $d$ -dimensional phonon dynamic in Monte Carlo simulations and measure the lifetimes of the metastable state. First, we summarize theoretical predictions for the lifetime. As  $T \rightarrow 0$ , the exact prediction [17,18] for the energy barrier between the metastable and stable states is given by

$$\Gamma(H, J) = 8J\ell_c - 2|H|(\ell_c^2 - \ell_c + 1) , \quad (7)$$

where the linear critical droplet size in units of the lattice constant is  $\ell_c = \lceil 2J/|H| \rceil$ , and  $\lceil x \rceil$  denotes the smallest integer not less than  $x$ . For example, for  $2J < |H| < 4J$ ,  $\ell_c = 1$ , and for  $J < |H| < 2J$ ,  $\ell_c = 2$ . (At  $|H| = 2$ , the critical droplet size changes.) For  $\ell_c > 1$ , the critical droplet is a cluster of overturned spins, which is an  $\ell_c \times (\ell_c - 1)$  rectangle with one additional overturned spin on one of its long sides. For  $\ell_c = 1$ , a single overturned spin is the critical droplet. This formula is valid only when  $2J/|H|$  is not an integer and  $|H| < 4J$ . At low temperatures the lifetime is the inverse of the probability of escaping from the metastable well, which can be written as

$$\langle \tau \rangle = A(H, T) \exp(\Gamma/T) , \quad (8)$$

where  $A(H, T)$  is the prefactor. We measure  $\langle \tau \rangle$  in units of Monte Carlo spin-flip attempts (MCS). (For the single-droplet decay mode considered here,  $\langle \tau \rangle$  is independent of the system

size if measured in MCS [3,19].) Hereafter, the field  $H$  and temperature  $T$  are given in units of  $J$ , and we set  $J = 1$ .

As  $T \rightarrow 0$ , we can calculate analytically [6] the prefactor  $A$  as a function of the field with the  $d$ -dimensional phonon dynamic, using absorbing Markov chains (AMC) [9,20]. For  $2 < |H| < 4$ ,

$$A(H, T \rightarrow 0, d) = \frac{4(2|H| - 4)^d + (8 - 2|H|)^d}{4(2|H| - 4)^d(8 - 2|H|)^d}. \quad (9)$$

For  $1 < |H| < 2$ ,

$$A(H, T \rightarrow 0, d) = \frac{|H|^d + 2(2 - |H|)^d}{2^{d+3}|H|^d(2 - |H|)^d}. \quad (10)$$

Near  $|H| = 2$ , both below and above, we find from Eqs. (9) and (10) that for  $|H|$  fixed,

$$\lim_{T \rightarrow 0, |H| \neq 2} A(H, T, d) = \frac{1}{C_1 ||H| - 2|^d}, \quad (11)$$

where  $C_1 = 2^{d+2}$  for  $|H| > 2$  and  $C_1 = 2^{d+3}$  for  $|H| < 2$ . On the other hand, as  $|H| \rightarrow 2^\pm$  at nonzero  $T$ , with the  $d$ -dimensional phonon dynamic, the transition rate,  $W_{km}$  [Eq. (6)], approaches  $T||H| - 2|^{d-1}$  times a constant. Since the transition rate is inversely proportional to the prefactor, we find that for  $T$  fixed,

$$\lim_{|H| \rightarrow 2^\pm, T > 0} A(H, T, d) = \frac{C_2}{T||H| - 2|^{d-1}}, \quad (12)$$

where the constant  $C_2$  may depend on  $d$ . The exact value of  $C_2$  could not be obtained analytically, so we examine it numerically (at the end of Sec. IV). As  $|H| \rightarrow 2^\pm$ , for  $d = 1$  the prefactor approaches  $C_2/T$  so that there is no field dependence, but for  $d = 2$  and 3 the prefactor diverges as  $C_2/(T||H| - 2|)$  and  $C_2/(T||H| - 2|^2)$ , respectively.

To investigate the region in which Eqs. (11) and (12) are applicable, and to examine whether there is any scaling behavior in the prefactor near  $|H| = 2$  and  $T = 0$ , we performed Monte Carlo simulations with absorbing Markov chains (MCAMC) [9,20] near  $|H| = 2$  at low temperatures, using the  $d$ -dimensional phonon dynamic [Eq. (6)]. Average lifetimes were measured over 2000 escapes with the linear system size  $L = 24$  and periodic boundary

conditions. Since this system size is much larger than the critical droplet size near  $|H| = 2$ , the dynamic behavior of the system does not depend on the examined system size. (This was confirmed by comparing with simulations for  $L = 48$ .) The range of temperatures examined was between  $T = 0.006$  and  $T = 0.10$ , and the range of fields used was from  $|H| - 2 = \pm 10^{-5}$  to  $|H| - 2 = \pm 0.3$ . At significantly low temperatures in a particular field or in a field quite close to  $|H| = 2$  at a particular temperature, the MPFUN package [21] was used for arbitrarily high-precision calculations. Eq. (8) was used to obtain the prefactor from the measured average lifetimes.

Figure 2 illustrates the analytic and numerical (Monte Carlo simulations at  $T = 0.1$ ) prefactors as functions of the field with the Glauber and the  $d$ -dimensional phonon dynamics. The analytic results for the prefactor with the phonon dynamics diverge as  $|H| \rightarrow 2^\pm$ . This divergence does not occur with the Glauber dynamic (straight solid lines in Fig. 2). The simulation data at  $T = 0.1$  agree well with the analytic results far away from  $|H| = 2$ , but they start to deviate from the analytic results as  $|H|$  approaches 2. This deviation is more significant for lower-dimensional phonon baths (smaller  $d$ ) at a fixed temperature, as shown in Fig. 2. For  $d = 3$  the simulation data at  $T = 0.1$  deviate from the analytic results only when the field is much closer to 2 than for the  $d = 1$  simulation data. We also find that lower-dimensional phonon dynamics need much lower temperatures to agree with the analytic results as  $|H|$  approaches 2. From now on, we concentrate on the phonon dynamics only.

Figure 3 shows log-log plots of the prefactor as a function of field at different temperatures and for different  $d$ . For  $d = 1, 2$ , and 3, the simulation data show two regimes where Eqs. (11) and (12) hold, respectively. Roughly speaking (more precise statements will be made in Sec. V.), when the field is not too close to  $|H| = 2$  [about the right halves of Figs. 3 (a), (b), and (c)], below (or above)  $|H| = 2$ , the prefactors at different temperatures converge to a linear curve. For  $d = 1$ , these converging linear curves can be found for larger  $||H| - 2|$  at higher  $T$ . The slopes of the converging linear curves (this is easily seen for  $d = 2$  and 3) are approximately  $-d$ , as expected from Eq. (11). When the field is close enough to

$|H| = 2$  (the left halves of Fig. 3), the prefactor at fixed temperature again behaves linearly with  $||H| - 2|$  on a logarithmic scale. As expected from Eq. (12), the slopes of those linear curves are approximately  $-(d - 1)$  and do not depend on temperature, but the intercepts are different for different temperatures.

#### IV. SCALING

Assuming that the prefactor  $A$  is a generalized homogeneous function [22] of the field and temperature only, we can write it as

$$A(\lambda^{a_h} h, \lambda^{a_T} T) = \lambda^{a_A} A(h, T), \quad (13)$$

where  $h = |H| - 2$ . Choosing  $\lambda = T^{-1/a_T}$ , this gives

$$A(h, T) = \left(\frac{1}{T}\right)^{a_A/a_T} \Phi^\pm\left(\frac{h}{T^{a_h/a_T}}\right), \quad (14)$$

where  $\Phi^\pm(x)$  are scaling functions for  $x = h/T^{a_h/a_T} > 0$  and  $x < 0$ , respectively. Since the prefactor has the asymptotic behaviors shown in Eqs. (11) and (12), the scaling functions  $\Phi^\pm(x)$  should have these properties:

$$\lim_{|x| \rightarrow \infty} \Phi^\pm(x) = \frac{1}{C_1 |x|^d}, \quad \lim_{|x| \rightarrow 0} \Phi^\pm(x) = \frac{C_2}{|x|^{d-1}}. \quad (15)$$

From the above properties, the scaling exponents are determined to be  $a_A/a_T = d$  and  $a_h/a_T = 1$ , so  $A(h, T) = (1/T)^d \Phi^\pm(h/T)$ .

If we rewrite the prefactor using scaling functions,  $\Psi^\pm(x) = |x|^{d-1} \Phi^\pm(x)$ , which have these properties

$$\lim_{|x| \rightarrow \infty} \Psi^\pm(x) = \frac{1}{C_1 |x|}, \quad \lim_{|x| \rightarrow 0} \Psi^\pm(x) = C_2, \quad (16)$$

then the prefactor can be written as

$$A(h, T) = \frac{1}{T} \frac{1}{h^{d-1}} \Psi^\pm\left(\frac{h}{T}\right). \quad (17)$$

Log-log plots of  $T|h|^{d-1}A$  vs  $|h|/T$  at different temperatures and for different  $d$  are shown in Fig. 4. The simulation data for different temperatures collapse well onto each other for each value of  $d$  and for  $|H| > 2$  (or  $|H| < 2$ ). Because  $C_1$  for a particular  $d$  and  $|H| < 2$  is the same as  $C_1$  for  $d+1$  and  $|H| > 2$  [Eqs. (11) and (16)], the simulation data in the regime of large  $|h|/T$  for  $d$  and  $|H| < 2$  fall on the data for  $d+1$  and  $|H| > 2$ . Using the fact that for large  $|h|/T$  and  $|H| > 2$  ( $|H| < 2$ ),  $C_1$  multiplied by  $2^d$  for  $d$  is the same as  $C_1$  for  $d+1$ , we make log-log plots of  $T|h|^{d-1}A$  multiplied by  $2^d$  vs  $|h|/T$  for different temperatures and for different  $d$  (see Fig. 5). Then all the simulation data for different temperatures and different  $d$  collapse well onto two master curves, one for  $|H| > 2$ , and the other for  $|H| < 2$ . The saturation value of  $2^d T|h|^{d-1}A$  as  $|h|/T \rightarrow 0$  ( $2^d C_2$ ) is approximately  $2/3$  (we do not know if this value is exactly  $2/3$  or not), so that  $C_2 \approx 2/3 \cdot 1/2^d$  and  $C_2 \propto 1/C_1$ . Using this approximate expression for  $C_2$  and Eqs. (16) and (17), we can confirm that the slopes of the log-log plots of  $2^d T|h|^{d-1}A$  vs  $x = |h|/T$  (Fig. 5) for large  $x$  are  $-1$  for both  $|H| > 2$  and  $|H| < 2$ , and that their intercepts at  $x = 1$  for  $|H| > 2$  ( $|H| < 2$ ) are approximately  $\log_{10}(1/4)$  ( $\log_{10}(1/8)$ ).

## V. DISCUSSION AND CONCLUSIONS

Our results indicate that the divergence of the lifetime prefactor is caused by the phonon dynamic we imposed, not by any unusual properties of the saddle points themselves, as is the case for Ref. [11]. Referring to Fig. 6, we discuss saddle points and the most probable paths to escape from the metastable state for different fields.

For  $|H| > 2$ , the saddle point corresponds to the configuration SA, only one overturned spin, so the most probable path to escape from the metastable well is A→SA. As  $|H| \rightarrow 2^+$ , the energy difference between SA and C approaches zero (Fig. 6), so the transition rate between them becomes zero. Consequently, the attempt frequency to grow the droplet along the downhill path SA→C decreases. This is the reason that the lifetime prefactor diverges as  $|H| \rightarrow 2^+$ . Then, a new probable path towards SC through SA begins to be

preferred to the downhill path. At  $|H| = 2$ , the path SA→C is forbidden, and the most probable path is directed towards the saddle point SC.

For  $|H| < 2$ , the saddle point corresponds to the configuration SB, an L-shaped cluster of three overturned spins. For this field, the most probable path to escape from the metastable well is A→SA→C→SB. As  $|H| \rightarrow 2^-$ , the energy difference between SA and C and the energy difference between C and SB both approach zero, so that the transition rates between them become zero. As a result, the attempt frequency along the most probable path towards the saddle point SB decreases, which leads to the prefactor divergence as  $|H| \rightarrow 2^-$ . Then, a new probable path towards SC through SA develops (Fig. 6). Thus, SC starts to compete with SB. At  $|H| = 2$ , the attempt frequency towards SB is zero, and the most probable path is towards the saddle point SC.

The previously shown scaling behavior of the prefactor can be observed from the simulation data in Fig. 3. In the log-log plots of  $A$  vs  $||H| - 2|$ , a slope of  $-(d - 1)$  is found for the regime when  $||H| - 2|/T \rightarrow 0$ , while a slope of  $-d$  is found when  $||H| - 2|/T \rightarrow \infty$ . The variable  $||H| - 2|/T$  (not simply either  $||H| - 2|$  or  $T$ ) determines how those two regimes change with field and temperature. The slope of  $-(d - 1)$  occurs at smaller  $||H| - 2|$  at lower temperatures, in order to reduce  $||H| - 2|/T$ , compared to higher-temperature data. The slope of  $-d$  occurs at larger  $||H| - 2|$  at higher temperatures, in order to increase  $||H| - 2|/T$ , compared to lower-temperature data.

In summary, we examined the prefactor of the lifetime of the metastable state for a square-lattice Ising ferromagnet with a  $d$ -dimensional phonon bath attached to each spin. Using the transition rates calculated from the density-matrix equation, we demonstrated analytically and numerically that the metastable lifetime prefactor diverges as  $|H| \rightarrow 2$ , and that it also scales as a function of  $||H| - 2|/T$  for each value of  $d$ , near  $|H| = 2$  and  $T = 0$ . This scaling is a result of the fact that the prefactor is a generalized homogeneous function [22] of the field and temperature. The divergence and scaling of the prefactor are due to the chosen dynamic, not to any non-smooth energy landscape at the particular magnetic field.

### **Acknowledgments**

This work was funded by NSF Grant Nos. DMR-9871455 and DMR-0120310, and by Florida State University through the School of Computational Science and Information Technology and the Center for Materials Research and Technology.

## REFERENCES

\* Electronic address: park@csit.fsu.edu

† Electronic address: man40@ra.msstate.edu

‡ Electronic address: rikvold@csit.fsu.edu

- [1] F. F. Abraham, *Homogeneous Nucleation Theory* (Academic, New York, 1974).
- [2] D. W. Oxtoby, J. Phys.: Condens. Matt. **4**, 7627 (1992).
- [3] P. A. Rikvold and B. M. Gorman, in *Annual Reviews of Computational Physics I*, edited by D. Stauffer (World Scientific, Singapore, 1994), p.149.
- [4] A. J. Leggett, Phys. Rev. Lett. **53**, 1096 (1984).
- [5] K. Park and M. A. Novotny, in *Computer Simulation Studies in Condensed Matter Physics XIV*, edited by D. P. Landau, S. P. Lewis, and H.-B. Schüttler, (Springer-Verlag, Berlin Heidelberg, in press).
- [6] K. Park and M. A. Novotny, Comp. Phys. Comm., in press.; e-print cond-mat/0109214 (unpublished).
- [7] R. J. Glauber, J. Math. Phys. **4**, 294 (1963).
- [8] P. A. Martin, J. Stat. Phys. **16**, 149 (1977).
- [9] M. A. Novotny, in *Computer Simulation Studies in Condensed Matter Physics IX*, ed. by D. P. Landau, K. K. Mon, and H.-B. Shüttler (Springer-Verlag, Berlin Heidelberg, 1997).
- [10] M. A. Novotny, in *Computer Simulation Studies in Condensed Matter Physics XV*, edited by D. P. Landau, S. P. Lewis, and H.-B. Schüttler, (Springer-Verlag, Berlin Heidelberg, in press).
- [11] R. S. Maier and D. L. Stein, Phys. Rev. Lett. **87**, 270601 (2001).

- [12] R. S. Maier and D. L. Stein, *J. Stat. Phys.* **83**, 291 (1996).
- [13] V. A. Shneidman and G. M. Nita, e-print cond-mat/0201064 (unpublished).
- [14] F. Hartmann-Boutron, P. Politi, and J. Villain, *Int. J. Mod. Phys. B* **10**, 2577 (1996);  
A. Fort, A. Rettori, J. Villain, D. Gatteschi, and R. Sessoli, *Phys. Rev. Lett.* **80**, 612 (1998).
- [15] K. Blum, *Density Matrix Theory and Applications*, 2nd edn. (Plenum Press, New York, 1996), Chapter 8.
- [16] M. N. Leuenberger and D. Loss, *Phys. Rev. B* **61**, 1286 (2000).
- [17] E. Jordão Neves and R. H. Schonmann, *Commun. Math. Phys.* **137**, 209 (1991).
- [18] A. Bovier and F. Manzo, *J. Stat. Phys.* **107**, 757 (2002).
- [19] P. A. Rikvold, H. Tomita, S. Miyashita, and S. W. Side, *Phys. Rev. E* **49**, 5080 (1994).
- [20] M. A. Novotny, in *Annual Reviews of Computational Physics IX*, edited by D. Stauffer (World Scientific, Singapore, 2001) pp. 153-210.
- [21] D. H. Bailey, *ACM Trans. Math. Software* **21**, 379 (1995).
- [22] A. Hankey and H. E. Stanley, *Phys. Rev. B* **6**, 3515 (1972).

## FIGURES

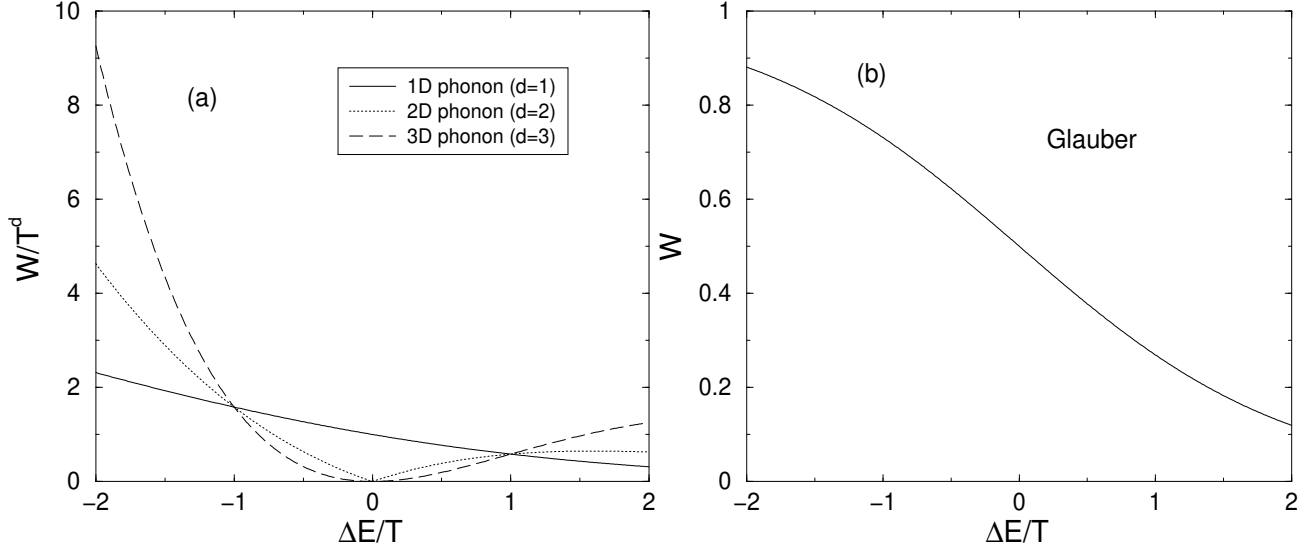


FIG. 1. (a) Transition rate  $W$  divided by  $T^d$  vs the energy difference  $\Delta E$  scaled by  $T$  for the  $d$ -dimensional phonon dynamics. (We use units such as  $k_B = 1$ .) Here we ignore the proportionality constant in  $W$ , setting  $\lambda^2/\Theta\eta\hbar^{d+1}c^{d+2} = 1$ . (b) Transition rate  $W$  vs  $\Delta E/T$  for the Glauber dynamic.

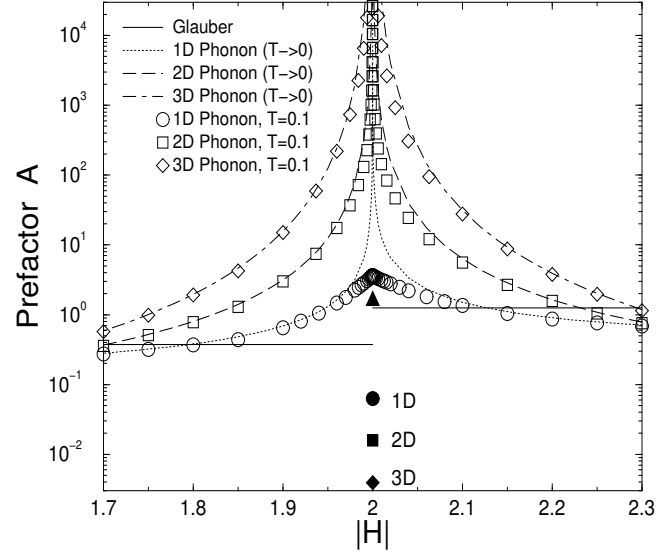


FIG. 2. The prefactor  $A$  vs field  $|H|$  for the Glauber dynamic and the  $d$ -dimensional phonon dynamics. The open symbols are from the Monte Carlo simulations at  $T = 0.1$  with the phonon dynamics. The curves are from the low-temperature analytic results Eqs. (9) and (10) with the phonon dynamics, while the straight solid lines are for the Glauber dynamic. For the  $d = 1$  simulation data with the phonon dynamic, a lower temperature or a field farther away from  $|H| = 2$  is needed to agree with the analytic results, compared to the simulation data for higher  $d$ . At  $|H| = 2$ , the critical droplet size changes, so the theoretical prediction Eq. (7) is not valid. The filled symbols are from the Monte Carlo simulations with the phonon dynamics at  $|H| = 2$ , except for the filled triangle, which is from the Glauber dynamic.

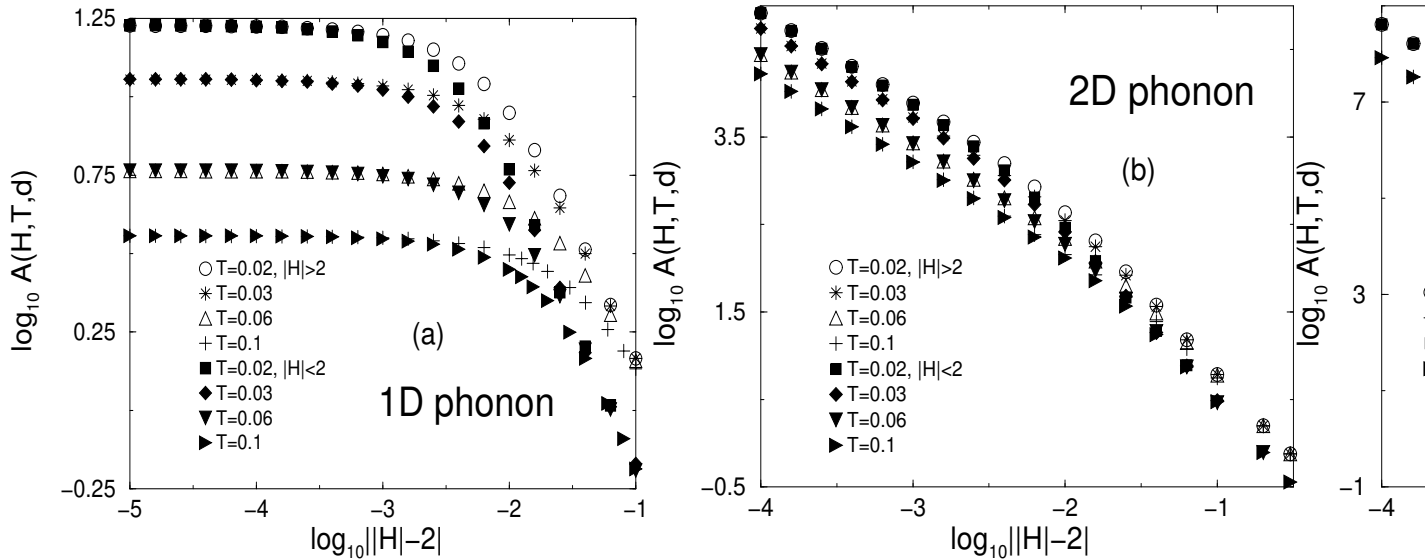


FIG. 3. Log-log plots of the prefactor  $A(H, T, d)$  vs  $|H| - 2$  at different temperatures for (a)  $d = 1$ , (b)  $d = 2$ , and (c)  $d = 3$  dimensional phonon dynamics, as the field  $|H|$  approaches 2 from above (empty symbols) and below (filled symbols). In (c), only data for two temperatures are shown for clarity, while the simulations were performed for  $T = 0.01, 0.02, 0.03, 0.06$ , and  $0.1$ . There are two regimes in these plots: (1) As  $|H| - 2|/T \rightarrow 0$  (the left-hand side of the plots), the slopes of the linear curves for different temperatures become  $-(d - 1)$ . (2) As  $|H| - 2|/T \rightarrow \infty$  (the right-hand side of the plots), the curves for different temperatures collapse onto single linear curves whose slopes are  $-d$ . These results are predicted from Eqs. (11) and (12).

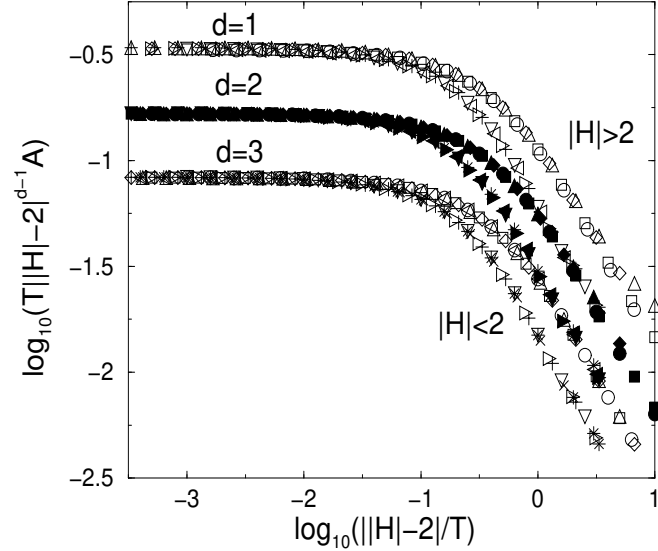


FIG. 4. Log-log plots of  $T|H| - 2|^{d-1}A(H, T, d)$  vs  $x = |H| - 2|/T$  for different temperatures (for  $d = 1$ ,  $T = 0.006, 0.01, 0.02, 0.03$ , for  $d = 2$ ,  $T = 0.02, 0.03, 0.04, 0.06$ , and for  $d = 3$ ,  $T = 0.01, 0.02, 0.03, 0.06, 0.1$ ) and different-dimensional phonon dynamics. For each value of  $d$ , the upper curves are for  $|H| > 2$ , while the lower curves are for  $|H| < 2$ . The simulation data for different temperatures collapse well for each value of  $d$ . Also, for large  $x$ , the curves for  $d$  and  $|H| < 2$  coincide with those for  $d + 1$  and  $|H| > 2$ , and the curves multiplied by 2 for  $d + 1$  and  $|H| > 2$  ( $|H| < 2$ ) coincide with the curves for  $d$  and  $|H| > 2$  ( $|H| < 2$ ).

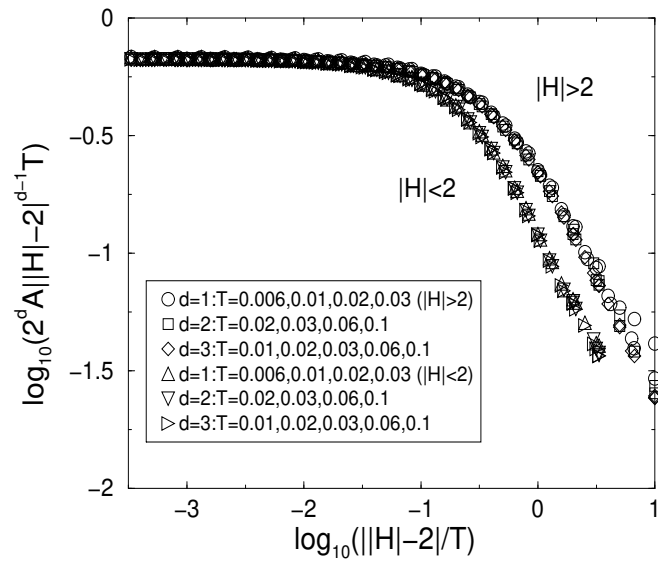


FIG. 5. Log-log plots of  $T||H| - 2|^{d-1}A(H, T, d)$  multiplied by  $2^d$  vs  $||H| - 2|/T$  for different  $T$  and  $d$ . For  $|H| > 2$  (or  $|H| < 2$ ), all the simulation data for different  $T$  and  $d$  collapse onto a single curve. The scaling function for  $|H| > 2$  is different from that for  $|H| < 2$ . Here the saturation value of  $2^d T ||H| - 2|^{d-1}A(H, T)$  as  $||H| - 2|/T \rightarrow 0$  (that is,  $2^d C_2$ ) is approximately  $2/3$ , so that  $C_2 \approx 2/3 \cdot 1/2^d$ .

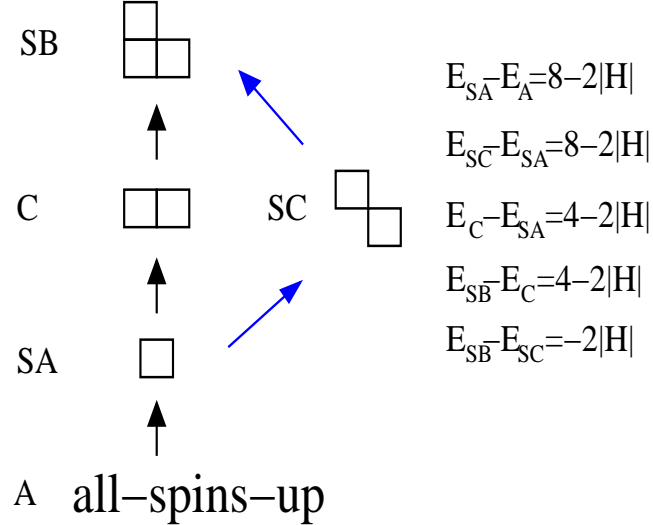


FIG. 6. Schematic diagram that shows the most probable paths of the system for different fields. Each box represents one overturned spin. Each configuration is labeled. The configuration labeled SA is the saddle point for  $|H| > 2$ , SB for  $|H| < 2$ , and SC for  $|H| = 2$ . The energy difference between two configurations is given on the right-hand side. As shown, the energy difference between SA and C is zero at  $|H| = 2$ , and so is the energy difference between C and SB. Therefore, at  $|H| = 2$ , the path from SA to SB through C is forbidden according to the phonon dynamic, Eq. (6). Consequently, the system chooses the saddle point SC to reach the configuration SB (A $\rightarrow$ SA $\rightarrow$ SC $\rightarrow$ SB). Then the energy barrier at  $|H| = 2$  is  $E_{SC} - E_A = 2(8 - 2|H|) = 8$  since the path from SC to SB is downhill.